IEEE Access
Multidisciplinary | Rapid Review | Open Access Journal

Received August 15, 2020, accepted August 28, 2020, date of publication August 31, 2020, date of current version September 14, 2020.

Digital Object Identifier 10.1109/ACCESS.2020.3020631

Graphene-Integrated Plasmonics Metasurface for Active Controlling Artificial Second Harmonic Generation

KAI GUO[1,2], ZIXIANG LI[1], AND ZHONGYI GUO[1,2]
[1]School of Computer and Information, Hefei University of Technology, Hefei 230009, China
[2]State Key Laboratory of Millimeter Waves, Southeast University, Nanjing 210096, China

Corresponding author: Zhongyi Guo (guozhongyi@hfut.edu.cn)

This work was supported in part by the National Natural Science Foundation of China under Grant 61775050 and Grant 11804073, in part by the Fundamental Research Funds for the Central Universities under Grant PA2019GDZC0098, and in part by the State Key Laboratory of Millimeter Waves under Grant K201915.

ABSTRACT Plasmonics has developed tremendously in recent years owing to its significant performance in enhanced nonlinear optical emission. However, plasmonic structures have predefined geometry, lacking flexibility for active control of the artificial nonlinear signal. In this paper, we numerically investigate active control of second harmonic generation (SHG) from plasmonic metasurface based on magnetic Lorentz force. The unit element of designed plasmonic metasurface consists of a gold split ring resonator and a bismuth bar, and integrated with graphene layer. By varying the Fermi energy of graphene from 0.2 eV to 1.0 eV, we achieve a 17.2 THz shift of the second harmonic frequency. In addition, it is demonstrated that the range of SHG frequency shift can be further enlarged by increasing the number of graphene layer. Our results pave the way for applications in generation of continuous laser source, optical communications and signal processing.

INDEX TERMS Active control, artificial nonlineaity, plasmonic.

I. INTRODUCTION

In the framework of nonlinear optics, the induced polarization intensity depends on the strength of light-matter interaction, which is determined by the incident electric field and the linear and nonlinear optical susceptibilities [1]. Usually, nonlinear emission is limited to natural nonlinear materials. Thanks to the developments of metamaterials and metasurfaces, artificial nonlinearity offers new opportunities to go beyond the limitations of natural nonlinear materials [2]–[4].

During the past decade, tremendous advances have already been made in nonlinear metamaterials and metasurfaces [2]–[9]. Among them, second harmonic generation (SHG) from plasmonic metasurfaces has triggered significant research interest for two reasons [5], [10]. The first is that the second-order nonlinearities, such as SHG, are usually stronger than that the high-order cases, making it easier to be observed and utilized. The second is that these second-order processes are indeed forbidden within the electric dipole approximation in centrosymmetric materials such as noble metals. It is in contradiction to both theoretical and experimental results of enhanced SHG effects from plasmonic nanostructures [11]–[15]. According to hydrodynamic model, this SHG can be clarified into nonlinear Coulomb term, magnetic Lorentz force contribution, convective terms and so on [11], [16]. To promote the plasmonic SHG efficiency, a variety of metamaterial configurations have been designed based on different physical mechanism, which could be divided into two aspects. The main aspect is to increase the surface contributions from the enhanced near-field intensity by exciting strong electromagnetic resonances in metamaterials. To this end, Mie resonances [17]–[19], lattice resonance [20]–[22], and mode matching methods [23], [24] have been utilized. The other aspect of this improved SHG comes from the magnetic Lorentz force contribution [25], [26], which has been neglected due to weak magnetic response of conventional optical materials [27], [28] and slow drift velocity of electrons. By engineering metamaterials structure, electric and magnetic responses can be enhanced simultaneously, resulting in pronounced magnetic Lorentz force contributed SHG emission [25], [26], [29]. Nevertheless, little has been reported about continuously tunable SHG emission, which is an important issue for generation of light source.

The associate editor coordinating the review of this manuscript and approving it for publication was Lin Peng.

Most of the developed metamaterials so far are passive and their performances are fixed after fabrication, hindering their application in miniaturized and integrated optical systems. Recently, the concept of tunable metamaterials has been established to control the optical properties though different mechanisms, including mechanically stretchable system [30], semiconductors [31], and phase change materials [32]. Among them, graphene is of particular interests owing to the remarkable electrical and optical properties which mainly originate from exceptional Dirac cone-type band structure [33]–[36]. Compared with other method, graphene provides the gate voltage tenability of metamaterials with short response time and subwavelength interaction with electromagnetic field. Therefore, it has recently attracted considerable attention for its enormous applications of graphene in tunable metamaterials [33]–[35] and metasurfaces [37]–[42], such as electrically switchable cloaking devices [43], beam-steering in far field [44], tunable electromagnetically induced transparency [45], tunable-metamaterials for sensing [46], and tunable third-harmonic generation [47]–[49]. More importantly, the sensitivity of Fermi energy to the carrier density in the Dirac fermions results in ultrawide tunable space in responding external light fields, making it a feasible and outstanding platform for actively controllable plasmonics, especially at terahertz and far-infrared frequencies [50]. Recently, Xiao *et al.* proposed a strategy for active control of SHG in a plasmonic Fano structure by electrically doping its underlying monolayer graphene [51], in which the SHG emission comes from the surface contribution from metal.

In this work, we design a tunable artificial SHG from plasmonic metasurface integrated with graphene layer. Here, we employ the plasmonic metasurface described in [25], providing the artificial SHG effect based on magnetic Lorentz force. The integrated graphene layer provides the active tunability. Numerical simulation results show that the frequency of SHG emission can be tuned over 6 THz when a single layer graphene is placed below the plasmonic metasurface at a distance of 30 nm. In addition, it is demonstrated that the frequency of SHG emission could be tuned over an extended range of 17.2 THz, when the distance between graphene and metasurface is 0. We also show that the tunable range of SHG emission frequency could be increased further by introducing multiplayer graphene.

II. THEORETICAL MODELS

A. MODEL OF SHG

Figure 1(a) gives an overview of the tunable SHG emission, coming from the plasmonic metasurface integrated with graphene layer. Figures 1(b) and 1(c) show the schematic of a unit cell of the proposed tunable nanostructure. With the normal incidence of an x-polarized electromagnetic (EM) wave propagating along the z-direction, a circulating current can be induced in the gold split ring resonator, providing a strong magnetic field along the z-direction. The bismuth bars are considered as the sources of high drift velocity electrons,

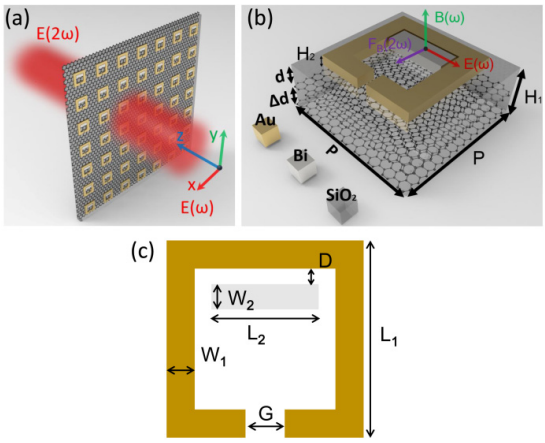

FIGURE 1. (a) Schematic of the SHG emission from metasurface integrated with graphene layer. (b) Side and (c) top views of a unit-cell marked with geometry parameters, which are $P = 1400$ nm, $H_1 = 500$ nm, $H_2 = 100$ nm, $G = 100$ nm, $W_1 = 180$ nm, $W_2 = 200$ nm, $L_1 = 1000$ nm, $L_2 = 600$ nm and $D = 20$ nm.

which are simultaneously driven by the incident electric field along the x-direction and the generated magnetic field along the z-direction. Therefore, the total force applied to the free electrons in the bismuth bar is [25], [26]:

$$\begin{aligned}\mathbf{F}_{\text{total}} &= \mathbf{F}_{\text{E}} + \mathbf{F}_{\text{B}} \\ &= q\mathbf{E}(\omega)e^{-i\omega t} + q\mathbf{v} \times \mathbf{B}(\omega)e^{-i\omega t} + \text{c.c.} \\ &= q\mathbf{E}(\omega)e^{-i\omega t} + q\tilde{\mu}_e\mathbf{E}(\omega) \times \mathbf{B}(\omega)e^{-i2\omega t} + \text{c.c.} \quad (1)\end{aligned}$$

where q is elementary charge, t is time, $\mathbf{v}$ is the mobility of the free electrons, $\mathbf{E}(\omega)$ and $\mathbf{B}(\omega)$ are local electric and magnetic fields at angular frequency ω, respectively, c.c. means the complex conjugate. The exhibited magnetic Lorentz force contribution of $\mathbf{E}(\omega) \times \mathbf{B}(\omega)e^{-i2\omega t}$ clearly supplies the mechanism of the SHG. The cross-polarized effect happens during this SHG radiation. It is because the incident electric field and the induced magnetic field are along the x- and z-axis, respectively, the magnetic force drives the electrons in bismuth bar along y-axis. Thus, the SHG signal radiates along both $+z$ and $-z$ direction in the y-polarization.

It should be note that the bismuth is chosen due to its high conductivity and mobility. Indeed, the bismuth can be replaced by gold for simplify experimental fabrication, but the SHG would be weak. High conductivity of the gold split ring and high mobility of the cut wire would both benefit the SHG. The bismuth has mobility of 1100 $\text{cm}^2/(\text{V}\cdot\text{s})$ and gold has mobility of 29.5 $\text{cm}^2/(\text{V}\cdot\text{s})$ [25]. The mobility of gold is much smaller than bismuth. For high effectivity SHG, we should choose bismuth. We refer the reader to [25], [26] for more detailed derivation of the magnetic Lorentz force based SHG emission.

B. MODEL OF TUNABILITY FROM GRAPHENE

When graphene layers are integrated into such a plasmonic metasurface, a capacitive coupling between them can strongly affect the linear and nonlinear responses of the system to the optical fields. Therefore, an extra tunability of the SHG emission is introduced owing to the tunable surface

conductivity of graphene, which can be described by the Kubo formula [51]–[54]:

$$\sigma_g = \frac{ie^2\left(\omega + i\tau^{-1}\right)}{\pi\hbar^2}\left[\int_{-\infty}^{+\infty}\frac{|\varepsilon|}{\left(\omega + i\tau^{-1}\right)^2}\frac{\partial f_d(\varepsilon)}{\partial\varepsilon}d\varepsilon - \int_0^{+\infty}\frac{\partial f_d(-\varepsilon) - \partial f_d(\varepsilon)}{\left(\omega + i\tau^{-1}\right)^2 - 4(\varepsilon/\hbar)^2}d\varepsilon\right] \quad (2)$$

where $f_d = 1/[1 + e^{(\varepsilon - E_F)/(k_B T)}]$ is the Fermi-Dirac distribution, ε is the energy, E_F is the Fermi energy, T is the temperature, e is the electron charge, $\hbar$ is the reduced Planck's constant, k_B is the Boltzmann constant, ω is the angular frequency, and τ is the momentum relaxation time, which represents the loss mechanism due to the carrier intraband scattering.

In the mid-infrared range with $|E_F| \geq k_B T$, the surface conductivity of graphene could be approximately expressed as

$$\sigma_g = i\frac{e^2 k_B T}{\pi\hbar\left(\omega + i\tau^{-1}\right)}\left[\frac{E_F}{k_B T} + 2\ln\left(\exp\left(-\frac{E_F}{k_B T}\right) + 1\right)\right] + i\frac{e^2}{4\pi\hbar}\ln\left[\frac{2|E_F| - \hbar\left(\omega + i\tau^{-1}\right)}{2|E_F| + \hbar\left(\omega + i\tau^{-1}\right)}\right] \quad (3)$$

$T = 300$ K and $\tau = \mu E_F/ev_F^2$, $\mu = 10^4\,\mathrm{cm^2V^{-1}S^{-1}}$ and $v_F \approx 10^6$ m/s as the mobility and Fermi velocity, respectively. Considering the fact that a DC mobility of $\mu > 10^5\ \mathrm{cm^2V^{-1}S^{-1}}$ has been experimentally achieved in high-quality suspended graphene [55], the value of mobility we used here is practical. Nevertheless, the charged impurities and defects of graphene introduced during experiment is difficult to control, reducing the carrier mobility of graphene. For graphene with low quality, the light-matter interaction could be weak, restricting the tunable range of the SHG emission.

By treating the single layer graphene as an ultra-thin metal film, its equivalent permittivity can be written as [56]

$$\varepsilon_g = 1 + \frac{i\sigma_g\eta_0}{k_0 d_g} \quad (4)$$

where $\eta_0 \approx 377\ \Omega$ is the impedance of air, k_0 is the wavenumber of electromagnetic field in free space, and d_g is the thickness of the graphene layer, which is assumed to be 1 nm in our work. Although an anisotropic model of graphene is more accurate [57], [58], it may affect the absorption effect in graphene layer. The isotropic model is efficient for the tunable ability of graphene in the proposed structure.

C. NUMERICAL SIMULATIONS FOR LINEAR PROCESS

The electromagnetic response of the proposed structure was calculated using a home-built program which is based on finite-element method. The free tetrahedral mesh was used in all simulations. The maximum and minimum mesh sizes are 100nm and 10nm, respectively. Smaller mesh sizes have also been tried and there is no change in the simulated result. Therefore, the numerical simulation is well converged. The distance between graphene layer and gold split ring is d. Period of a unit cell is $P = 1400$ nm. The thickness of SiO_2 is $H_1 = 500$ nm. The arm length of gold split ring is $L_1 = 1000$ nm. The thickness of gold split ring and bismuth bar is $H_2 = 100$ nm. The gap of gold split ring is $G = 100$ nm. The width of gold split ring is $W_1 = 180$ nm. The length and width of bismuth bar are $L_2 = 600$ nm and $W_2 = 200$ nm, respectively. The gap between gold split ring and bismuth bar is $D = 20$ nm. These geometrical parameters are optimized to achieve high SHG emission in terahertz region.

In our simulations, the complex dielectric permittivity of gold and bismuth as a function of frequency was described by Drude model:

$$\varepsilon = 1 - \frac{\omega_p^2}{\omega^2 + i\gamma\omega} \quad (5)$$

where ω_p is plasma frequency, γ is collision frequency and ω is the angular frequency. For gold, its plasma frequency is $2\pi\times2175$ THz and its collision frequency is $2\pi\times6.5$ THz [59]. For bismuth, its collision frequency is $2\pi\times7.5$ THz [25]. The optical response of the graphene layer is described by the above theoretical model. The refractive index of SiO_2 substrate was set to be constant of 4.82+0.026i over the whole spectral range of interest [25].

A single unit cell of the array is modeled with periodic boundary conditions in lateral directions (along both the x- and y-axes). Perfect matched layers (PMLs) are utilized on the top and bottom boundaries of the unit cell to eliminate reflective waves from the boundaries. Port boundary conditions are placed at the interior boundaries of the PMLs, allowing for a plane wave source and extracting the scattering parameters. The absorption spectrums of the proposed structure at fundamental frequency are obtained by 1-*Reflection-Transmission*.

D. NUMERICAL SIMULATIONS FOR NONLINEAR PROCESS

When experiment data for the second harmonic susceptibility of nanostructure is unavailable, the Miller's rule has been adopted to incorporate the property of the second order nonlinearity [60], [61]. Nevertheless, we may not use Miller's rule in our analysis. It is because the theory model of Miller's rule only considers the contribution of electric dipole mode in nanostructures to the SHG emission. In our case, the SHG from magnetic Lorentz force involves magnetic dipole resonance, therefore making the Miller's rule fails. In the nonlinear process of our simulation, the electromagnetic responses of both gold and SiO_2 are the same as that in linear process. The bismuth in magnetic field is described by a complex anisotropic conductivity tensor based on Drude mode [25], [62]:

$$\widehat{\sigma}(\omega) = \tilde{\sigma}\begin{bmatrix} \frac{1}{1+(\mu_e\mathbf{B})^2} & -\frac{\mu_e\mathbf{B}}{1+(\mu_e\mathbf{B})^2} & 0 \\ \frac{\mu_e\mathbf{B}}{1+(\mu_e\mathbf{B})^2} & \frac{1}{1+(\mu_e\mathbf{B})^2} & 0 \\ 0 & 0 & 1 \end{bmatrix} \quad (6)$$

where $\tilde{\sigma} = \sigma_0/(1 - i\omega\gamma)$ and $\mu_e = \mu_{e0}/(1 - i\omega\gamma)$ are the optical conductivity and mobility at frequency ω, respectively. The direct current conductivity σ_0 and mobility μ_{e0} are modeled with $2.2 \times 10^5 \mathrm{S/m}$ and 1100 $\mathrm{cm^2/(V{\cdot}s)}$, respectively [30]. It can be seen from Eqs. (1) and (6) that the influence of magnetic fields on SHG is two-fold. First, the magnitudes of SHG radiation could be tailored by applying external magnetic field with different intensity. Second, different second-order nonlinearity would be generated when the frequency of magnetic field is different from that of incident electric field [63].

To calculate the SHG emission, we utilize scattering boundary conditions at the top and bottom boundaries of the unit cell allowing for a Gaussian pulsed plane wave source. The x-polarized Gaussian pulsed plane incident wave was defined by the electric field $\mathbf{E}= (E_x, 0, 0)$ and the expression of E_x is

$$E_x = E\cos(\omega t - k_0 z)\, e^{-\left(\frac{t-t_0}{\Delta t}\right)^2} \tag{7}$$

where E is the peak amplitude of the electric field, ω is the angular frequency, t is time, k_0 is the wavenumber at the frequency ω, z is the coordinate in z-axis, t_0 and Δt are the parameters describing the Gaussian pulse. The values used in the simulation are $E = 10^7 \mathrm{V/m}$, $t_0 = 800$ fs, $\Delta t = 300$ fs, and the total time of 2 ps was simulated with a step of 1 fs. The value of incident frequency ω is the magnetic resonance frequency. According to the theory model, nonlinear signal could be obtained at frequency of 2ω. We use a point probe to receive the transmission of the Gaussian pulsed plane wave interacted with the proposed nanostructure and get the frequency spectrums of these transmission by Fourier transformation. Note that, without losing generality, we only consider the SHG emission contributed from the magnetic Lorentz force effect, even though both gold and graphene could emit SHG signal according to the hydrodynamic model of free electrons. Here, we only consider the artificial nonlinearity of the metasurface for two reasons. The first is that we focus on the tunable SHG frequency rather the enhancement of emission. To this end, graphene layer could provide the active control of optical responses. The second is that graphene is a centrosymmetric material and its second-order nonlinearity is forbidden at normal incidence, which is used as incident condition in this work.

III. RESULTS AND DISCUSSION

Figure 2(a) shows the simulated absorption spectrums of this metasurface integrated with a graphene layer at fundamental wavelength. The distance between the metasurface and graphene layer is $d = 100$ nm. When the Fermi energy of graphene varies from 1.0 eV to 0.2 eV, the absorption peak blue shifts from 28 THz to 29.5 THz. This phenomenon indicates that the optical response of this metasurface can be controlled by varying the Fermi energy of graphene layer. The position of the bismuth bar has no significant influence on the absorption spectrum. To show the physical nature

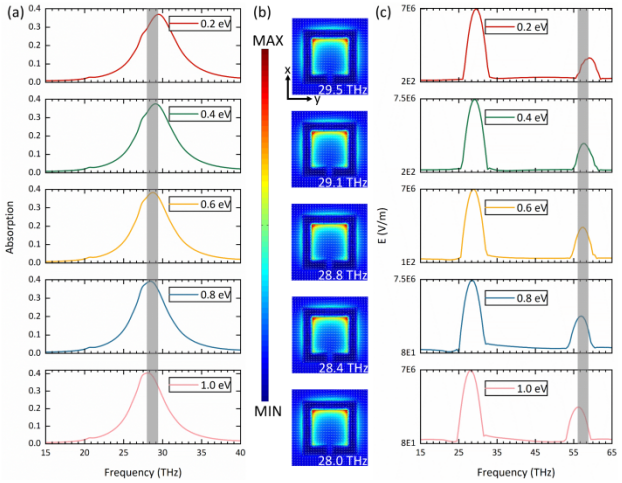

FIGURE 2. (a) Absorption of this metasurface when d=100nm, peaking at 28 THz, 28.4 THz, 28.8 THz, 29.1 THz and 29.5THz, when the Fermi energy of graphene is 1.0 eV, 0.8 eV, 0.6 eV, 0.4eV and 0.2 eV, respectively. (b) The normalized magnetic field distribution at the absorption peaks in (a). (c) The transmission in frequency domain. The SHG frequency shifts from 56 THz to 59 THz. The shadow represents frequency shift range.

of the absorption, Fig. 2(b) shows the surface currents and magnetic field distributions in the unit cell in the x-y plane at frequencies of 29.5 THz, 29.1 THz, 28.8 THz, 28.4 THz, and 28 THz, when the Fermi energy of graphene layer is 0.2 eV, 0.4 eV, 0.6 eV, 0.8 eV and 1.0 eV, respectively. We could observe circulating currents along the gold split ring resonator, producing the enhanced magnetic field. In addition, it is shown that the amounts of absorbed energy are almost constant. It means that the introduction of graphene layer has not change the intensities of magnetic field located inside the gold split ring. Since the SHG response is proportional to the intensity of magnetic field, we put the bismuth bar at the place where magnetic field is maximum. Figure 2(b) shows that the magnetic field is highly located near the arm of gold split ring, thus we put the bismuth bar there.

The transmission spectrum in time domain is calculated under the conditions of graphene layer with different Fermi energy of 0.2 eV, 0.4 eV, 0.6 eV, 0.8 eV and 1.0 eV (not shown here). These time spectrums are filtered and transformed to frequency spectrum by Fourier transformation, as shown in Fig. 2(c). The spectral purity of the SHG can be improved by increasing the total simulation time and reducing the time step, which may cost more simulation time and memory. Luckily, we can obviously see the SHG emission from current results. In each spectrum, the peaks at low and high frequencies correspond to fundamental and SHG frequency, respectively. The frequency of the fundamental peak shifts from 28 THz to 29.5 THz as the Fermi energy of graphene varying from 1.0 eV to 0.2 eV, being in a good agreement with the linear absorption spectrums. As a result, the SHG frequency can be tuned from 56 THz to 59 THz, covering a frequency range of 3 THz. This demonstrates the possibility of an efficient tuning of the SHG frequency from a metasurface by simple changing the Fermi energy of the integrated graphene layer.

It is worth to note that the graphene layer provides the tenability of SHG frequency owing to their tunable Fermi energy E_{F}. According to the relation between Fermi energy E_{F} and the charge-carrier density n, $E_F = \hbar\upsilon_F\sqrt{\pi\,|n|}$, we may tune the value of E_{F} via controlling the charge-carrier density in graphene layer, which could be realized by electrostatic doping and chemical doping methods, achieving high Fermi energy of $E_{\mathrm{F}} = 0.9$ eV [64] and $E_{\mathrm{F}} = 0.8$ eV [65], respectively. More importantly, a much higher value of Fermi energy $E_{\mathrm{F}} = 2.5$ eV has been experimentally obtained in photoexcited graphene layer [66]. These experiment results validate the above value of Fermi energy changing from 0 to 1eV is reasonable, and more importantly, the tunable range of SHG frequency may be enlarged further by using photoexcited graphene.

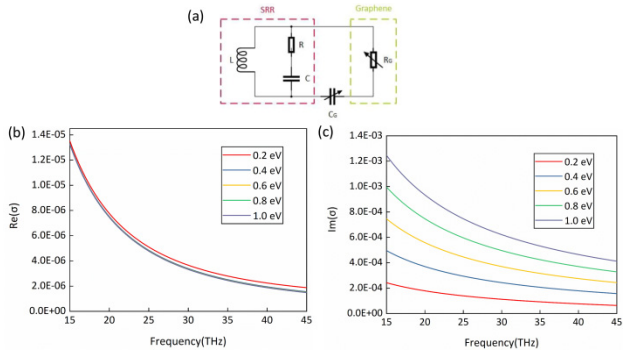

FIGURE 3. (a) Equivalent LC circuit model of the metasurface at magnetic resonance. (b) and (c) show the real part and imaginary part of conductivity of graphene, respectively.

The tuning of both fundamental and SHG frequencies can be predicted by an equivalent LC circuit model which is shown in Fig. 3(a). In this model, the metal ring and the split gap provide the inductance L and the capacitance C, respectively [67]. For the proposed metasurface integrated with a graphene layer, the capacitance can be expressed as $C = (\varepsilon_0\varepsilon_r S_1)\big/(4\pi gk)$, where ε_0 and ε_{r} represent the permittivity of vacuum and medium in the gap, respectively, κ is the extinction coefficient of gold, S_1 and g are the geometry parameters related to the gap, respectively. The resistor R represents the dissipation on the metal due to the electrical and radiation resistance. In addition, the graphene layer can be modeled by a sheet resistance $R_{\mathrm{G}} = 1\big/\sigma_{\mathrm{g}}$ and is capacitively coupled with the metasurface, where the coupling capacitance can be expressed as $C_{\mathrm{G}} = (\varepsilon\varepsilon_0)\big/d$, ε and ε_0 are the dielectric constant of the medium and free-space permittivity, respectively. According to the Kirchhoff's law, the resonance condition for the equivalent circuit requires

$$\omega = \left[\frac{C + C_{\mathrm{G}}}{2CC_{\mathrm{G}}RR_{\mathrm{G}}\,(C + C_{\mathrm{G}}) - R^2C^2C_{\mathrm{G}} - R_{\mathrm{G}}^2CC_{\mathrm{G}}^2}\right]^{\frac{1}{2}} \quad (8)$$

indicating that the resonance frequency of fundamental field can be actively tuned through the resistance of graphene layer and is also passively dependent on the distance between graphene layer and metasurface. It can be concluded when sheet resistance decreases (increases), the resonance frequency red (blue) shifts.

To explain the results in Fig. 2, we plot both the real and imaginary parts of the conductivity of the graphene layer, in Figs. 3 (b) and (c), as functions of its Fermi energy over a broadband frequency range from 15 THz to 45 THz. Even though the $\mathrm{Re}(\sigma_{\mathrm{g}})$ overlaps for the cases with 0.4eV to 1.0eV in Fig. 3(b), the value of $\mathrm{Im}(\sigma_{\mathrm{g}})$ increases with the Fermi energy, resulting in a decreased sheet resistance. Therefore, the frequencies of fundamental and SHG resonances blue shift from 28 THz to 29.5 THz and from 56 THz to 59 THz, respectively, when we vary the Fermi energy from 1.0eV to 0.2eV, as shown in Fig. 2. The simulation and theoretical results are in a good agreement with each other.

On the other hand, Eq. (8) reveals that the tunable range of both fundamental and SHG frequencies could be enlarged with the coupling capacitance. When the distance between graphene and gold split ring decreases, the coupling capacitance increases, and the tunable range of resonance frequencies will be amplified and is beneficial for the SHG emission. Therefore, to achieve a larger tunable range of SHG frequency, we may attempt to increase the capacitive coupling strength by squeezing the distance between the graphene layer and the proposed metasurface.

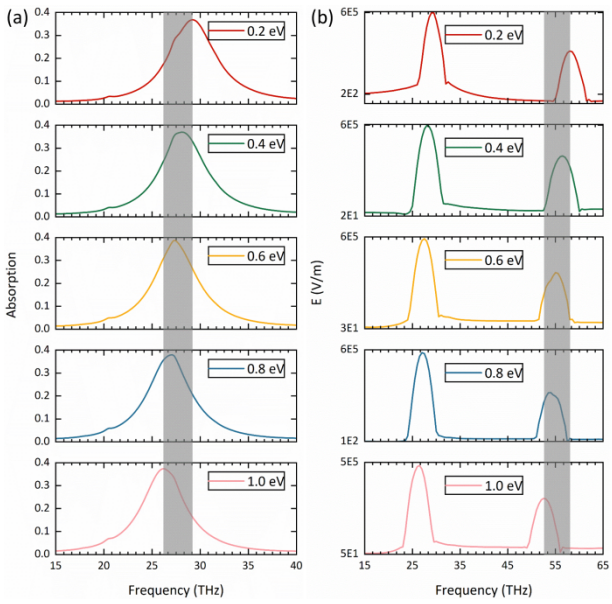

FIGURE 4. (a) Absorption of this metasurface when d=30 nm, peaking at 26.2 THz, 27 THz, 27.3 THz, 28.1 THz and 29.2 THz, when the Fermi energy of graphene is 1.0 eV, 0.8 eV, 0.6 eV, 0.4 eV and 0.2 eV, respectively. (b) The transmission in frequency domain. The peaks corresponding to SHG emission moves from 52.4 THz to 58.4 THz. The shadow represents frequency shift range.

To demonstrate, Fig. 4(a) shows the calculated linear absorption spectrums of this metasurface with $d = 30$ nm. The absorption peak shifts from 26.2 THz to 29.2 THz, following the Fermi energy of graphene varying from 1.0 eV to 0.2 eV. Figure 4(b) shows the transmission spectrums in frequency domain transformed from the time domain in logarithmic coordinate. In each spectrum, the peaks at low

and high frequencies correspond to fundamental and SHG fields, respectively. It could be seen that the tunable range of SHG frequency is extended to 6 THz, shifting from 52.4 THz to 58.4 THz. This shift range is bigger than the previous case in which $d = 100$ nm, validating the good performance of our proposed method.

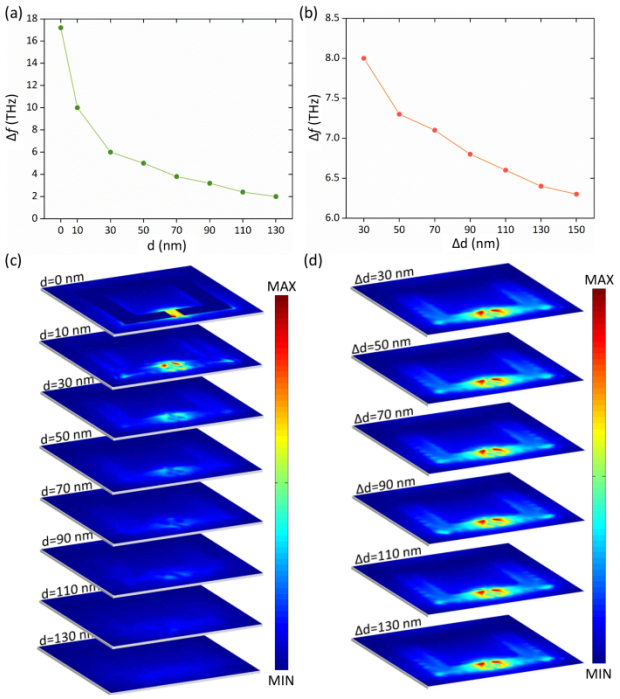

FIGURE 5. The tunable range of SHG frequency for the case with (a) one and (b) two layers of graphene, as functions of d and Δd, respectively. (c) and (d) show the electric field distribution in graphene layer in the x-y plane for the case with one and two layers of graphene, respectively. Here all electric fields are extracted from the first graphene layer.

Following the results above, we investigate the dependence of the tunable SHG frequency range emitted from the proposed structure on the distance between graphene layer and the metasurface, when the Fermi energy of graphene varies from 0 eV to 1.0 eV. Essentially, the plasmonic metasurface dominates its magnetic resonance and the graphene layer mildly influence this resonance by capacitively interacting with the metasurface. As shown in Fig. 5(a), the tunable frequency range Δf can be as high as 17.2 THz when the graphene layer is directly attached at the plasmonic metasurface ($d = 0$ nm). As the distance d increases, the value of Δf reduces very fast and approaches 2 THz when $d = 130$ nm, owing to fading away of the capacitive coupling between graphene layer and metasurface. Figure 5(c) plots the electric field distribution in graphene layer with different distance d in the x-y plane. The transferred energy from metasurface to graphene layer fades away with the distance d increasing, and almost disappears when $d = 130$ nm.

To investigate, the dependence of the tunable range of SHG frequency on the number of graphene layers is studied. Since the graphene layer brings the modulation of frequencies of both fundamental and SHG fields through capacitive coupling with the plasmonic metasurface, if more graphene layers are integrated to the proposed structure, we may further extend the tunable SHG frequency range. As a demonstration, we calculate Δf of the case with two layers of graphene, where the first layer is fixed at $d = 30$ nm below the metasurface and the second layer is located below the first one with different distances Δd from 30 nm to 150 nm. The dependence of Δf on Δd and the corresponding electric field distribution in the first graphene layer are plotted in Figs. 5(b) and 5(d), respectively. When $\Delta d = 30$ nm, the tunable range of SHG frequency $\Delta f = 8$ THz, which is significantly extended compared to the case of single graphene layer with $d = 30$ nm. What is more, a comparison between Fig. 5(a) and 5(b) shows that Δf indeed increases owing to the introduction of the second layer of graphene, further demonstrating the tunable SHG frequency by using our proposed method.

The above simulation results show when the distance between the plasmonic metasurface and the monolayer graphene is decreased from $d = 130$ nm to 0 nm, the tunable range of SHG frequency could extend from 2.0 THz to 17.2 THz. In addition, we have also demonstrated that the tunable range of SHG frequency could be improved by introducing more graphene layer. It is a pretty good result in comparison to some reported results [34] with respect to the working frequency and the linewidth, which could be beneficial for continuously generating terahertz light source. Although this work was complemented with numerical simulations, in the view of experiment, the preparation of the designed structure is highly feasible. Substrate with smooth surface and required thickness should be prepared at first. The large scale graphene could be synthesized on substrate through chemical vapor deposition, and another SiO_2 with smooth surface could cover the graphene film. Thus, the graphene film inside the SiO_2 substrate could be obtained. Defects during the fabrication need to be well minimized. In addition, the two-layer graphene could be obtained by stacking monolayer graphene [68]. These metal parts, gold and bismuth, could be deposited on substrate by electron-beam evaporation and magnetron sputtering. Then the metasurface could be conveniently manufactured in periodic lattice by microfabrication techniques with ultraviolet lithography. For measurement, the transmission (T) and reflection (R) spectrum can be obtained in experiment, and absorption spectrum can be calculated by 1-T-R.

IV. CONCLUSION

In this work, we have demonstrated a tunable SHG from plasmonic metasurface integrated with graphene layer, where the plasmonic metasurface and graphene layer offer the SHG emission and tunability, respectively. Numerical simulation results have demonstrated that the SHG frequency can be tuned over 6 THz when a single layer graphene is placed below the plasmonic metasurface at a distance of 30 nm. In addition, the tunable range of SHG frequency could be enlarged to 17.2 THz, when the distance between graphene

and metasurface is 0. We also show that the tunable range of SHG emission frequency could be increased further by introducing multiplayer graphene. The results in this study can be used to achieve tunable nonlinear metamaterials for practical application such as generation of light source.

REFERENCES

[1] Y. R. Shen, *The Principles of Nonlinear Optics*. New York, NY, USA: Wiley, 1984, p. 575.

[2] M. Lapine, I. V. Shadrivov, and Y. S. Kivshar, "Colloquium: Nonlinear metamaterials," *Rev. Mod. Phys.*, vol. 86, no. 3, pp. 1093–1123, Sep. 2014.

[3] A. Krasnok, M. Tymchenko, and A. Alú, "Nonlinear metasurfaces: A paradigm shift in nonlinear optics," *Mater. Today*, vol. 21, no. 1, pp. 8–21, Jan. 2018.

[4] G. Li, S. Zhang, and T. Zentgraf, "Nonlinear photonic metasurfaces," *Nature Rev. Mater.*, vol. 2, no. 5, p. 17010, Mar. 2017.

[5] J. Butet, P.-F. Brevet, and O. J. F. Martin, "Optical second harmonic generation in plasmonic nanostructures: From fundamental principles to advanced applications," *ACS Nano*, vol. 9, no. 11, pp. 10545–10562, Oct. 2015.

[6] D. A. Smirnova, A. E. Miroshnichenko, Y. S. Kivshar, and A. B. Khanikaev, "Tunable nonlinear graphene metasurfaces," *Phys. Rev. B, Condens. Matter*, vol. 92, no. 16, Oct. 2015, Art. no. 161406.

[7] A. E. Minovich, A. E. Miroshnichenko, A. Y. Bykov, T. V. Murzina, D. N. Neshev, and Y. S. Kivshar, "Functional and nonlinear optical metasurfaces," *Laser Photon. Rev.*, vol. 9, no. 2, pp. 195–213, Mar. 2015.

[8] H.-T. Chen, A. J. Taylor, and N. Yu, "A review of metasurfaces: Physics and applications," *Rep. Prog. Phys.*, vol. 79, no. 7, Jun. 2016, Art. no. 076401.

[9] F. Ding, A. Pors, and S. I. Bozhevolnyi, "Gradient metasurfaces: A review of fundamentals and applications," *Rep. Prog. Phys.*, vol. 81, no. 2, Dec. 2017, Art. no. 026401.

[10] J. Butet, S. Dutta-Gupta, and O. J. F. Martin, "Surface second-harmonic generation from coupled spherical plasmonic nanoparticles: Eigenmode analysis and symmetry properties," *Phys. Rev. B, Condens. Matter*, vol. 89, no. 24, Jun. 2014, Art. no. 245449.

[11] C. Ciracì, E. Poutrina, M. Scalora, and D. R. Smith, "Origin of second-harmonic generation enhancement in optical split-ring resonators," *Phys. Rev. B, Condens. Matter*, vol. 85, no. 20, May 2012, Art. no. 201403.

[12] K. Guo, C. Qian, Y. L. Zhang, and K. H. Fung, "Second harmonic generation manipulation enabled by electromagnetic coupling in bian-isotropic metamolecules," *Adv. Opt. Mater.*, vol. 6, no. 7, Feb. 2018, Art. no. 1701154.

[13] K. Guo, Y. L. Zhang, C. Qian, and K. H. Fung, "Electric dipole-quadrupole hybridization induced enhancement of second-harmonic generation in T-shaped plasmonic heterodimers," *Opt. Express*, vol. 26, no. 9, pp. 11984–11993, Mar. 2018.

[14] S.-D. Liu, E. S. P. Leong, G.-C. Li, Y. Hou, J. Deng, J. H. Teng, H. C. Ong, and D. Y. Lei, "Polarization-independent multiple fano resonances in plasmonic nonamers for multimode-matching enhanced multiband second-harmonic generation," *ACS Nano*, vol. 10, no. 1, pp. 1442–1453, Jan. 2016.

[15] W. C. Zhai, T. Z. Qiao, D. J. Cai, W. J. Wang, J. D. Chen, Z. H. Chen, and S. D. Liu, "Anticrossing double Fano resonances generated in metallic/dielectric hybrid nanostructures using nonradiative anapole modes for enhanced nonlinear optical effects," *Opt. Express*, vol. 24, no. 24, pp. 27858–27869, Nov. 2016.

[16] C. Ciraci, E. Poutrina, M. Scalora, and D. R. Smith, "Second-harmonic generation in metallic nanoparticles: Clarification of the role of the surface," *Phys. Rev. B, Condens. Matter*, vol. 86, no. 11, Sep. 2012, Art. no. 115451.

[17] D. Smirnova, A. I. Smirnov, and Y. S. Kivshar, "Multipolar second-harmonic generation by mie-resonant dielectric nanoparticles," *Phys. Rev. A, Gen. Phys.*, vol. 97, no. 1, Jan. 2018, Art. no. 013807.

[18] S. Kruk, M. Weismann, A. Y. Bykov, E. A. Mamonov, I. A. Kolmychek, T. Murzina, N. C. Panoiu, D. N. Neshev, and Y. S. Kivshar, "Enhanced magnetic second-harmonic generation from resonant metasurfaces," *ACS Photon.*, vol. 2, no. 8, pp. 1007–1012, Jul. 2015.

[19] D. J. Yang, S. J. Im, G. M. Pan, S. J. Ding, Z. J. Yang, Z. H. Hao, L. Zhou, and Q. Q. Wang, "Magnetic Fano resonance-induced second-harmonic generation enhancement in plasmonic metamolecule rings," *Nanoscale*, vol. 9, no. 18, pp. 6068–6075, May 2017.

[20] L. Michaeli, S. Keren-Zur, O. Avayu, H. Suchowski, and T. Ellenbogen, "Nonlinear surface lattice resonance in plasmonic nanoparticle arrays," *Phys. Rev. Lett.*, vol. 118, no. 24, Jun. 2017, Art. no. 243904.

[21] G. F. Walsh and L. D. Negro, "Enhanced second harmonic generation by photonic–plasmonic Fano-type coupling in nanoplasmonic arrays," *Nano Lett.*, vol. 13, no. 7, pp. 3111–3117, Jun. 2013.

[22] S. Linden, F. B. P. Niesler, J. Förstner, Y. Grynko, T. Meier, and M. Wegener, "Collective effects in second-harmonic generation from Split-Ring-Resonator arrays," *Phys. Rev. Lett.*, vol. 109, no. 1, Jul. 2012, Art. no. 015502.

[23] Z. Li, W. Liu, Z. Li, H. Cheng, S. Chen, and J. Tian, "Fano-resonance-based mode-matching hybrid metasurface for enhanced second-harmonic generation," *Opt. Lett.*, vol. 42, no. 16, pp. 3117–3120, Aug. 2017.

[24] M. Celebrano, X. Wu, M. Baselli, S. Großmann, P. Biagioni, A. Locatelli, C. De Angelis, G. Cerullo, R. Osellame, B. Hecht, L. Duò, F. Ciccacci, and M. Finazzi, "Mode matching in multiresonant plasmonic nanoantennas for enhanced second harmonic generation," *Nature Nanotechnol.*, vol. 10, no. 5, pp. 412–417, Apr. 2015.

[25] Y. Wen and J. Zhou, "Artificial nonlinearity generated from electromagnetic coupling metamolecule," *Phys. Rev. Lett.*, vol. 118, no. 16, Apr. 2017, Art. no. 167401.

[26] Z. Guo, Z. Li, and K. Guo, "The enhanced second-harmonic generation based on magnetic-lorentz-force effect," *Annalen der Phys.*, vol. 531, no. 4, Feb. 2019, Art. no. 1800470.

[27] X. Xiong, W.-H. Sun, Y.-J. Bao, R.-W. Peng, M. Wang, C. Sun, X. Lu, J. Shao, Z.-F. Li, and N.-B. Ming, "Switching the electric and magnetic responses in a metamaterial," *Phys. Rev. B, Condens. Matter*, vol. 80, no. 20, Nov. 2009, Art. no. 201105.

[28] F. Shafiei, F. Monticone, K. Q. Le, X.-X. Liu, T. Hartsfield, A. Alú, and X. Li, "A subwavelength plasmonic metamolecule exhibiting magnetic-based optical fano resonance," *Nature Nanotechnol.*, vol. 8, no. 2, pp. 95–99, Feb. 2013.

[29] E. Rahimi, H. Xu, B.-C. Choi, and R. Gordon, "Lorentz nanoplasmonics for nonlinear generation," *Nano Lett.*, vol. 18, no. 12, pp. 8030–8034, Dec. 2018.

[30] F. Zhang, S. Feng, K. Qiu, Z. Liu, Y. Fan, W. Zhang, Q. Zhao, and J. Zhou, "Mechanically stretchable and tunable metamaterial absorber," *Appl. Phys. Lett.*, vol. 106, no. 9, Mar. 2015, Art. no. 091907.

[31] J. Han, A. Lakhtakia, and C. W. Qiu, "Terahertz metamaterials with semiconductor split-ring resonators for magnetostatic tunability," *Opt. Express*, vol. 16, no. 19, pp. 14390–14396, 2008.

[32] J. Tian, Q. Li, J. Lu, and M. Qiu, "Reconfigurable all-dielectric antenna-based metasurface driven by multipolar resonances," *Opt. Express*, vol. 26, no. 18, pp. 23918–23925, Sep. 2018.

[33] W. Zhu, F. Xiao, M. Kang, D. Sikdar, and M. Premaratne, "Tunable terahertz left-handed metamaterial based on multi-layer graphene-dielectric composite," *Appl. Phys. Lett.*, vol. 104, no. 5, Feb. 2014, Art. no. 051902.

[34] L. Ye, X. Chen, G. Cai, J. Zhu, N. Liu, and Q. Liu, "Electrically tunable broadband terahertz absorption with hybrid-patterned graphene metasurfaces," *Nanomaterials*, vol. 8, no. 8, p. 562, Jul. 2018.

[35] L. Ye, F. Zeng, Y. Zhang, and Q. H. Liu, "Composite graphene-metal microstructures for enhanced multiband absorption covering the entire terahertz range," *Carbon*, vol. 148, pp. 317–325, Jul. 2019.

[36] L. Luo, K. Wang, C. Ge, K. Guo, F. Shen, Z. Yin, and Z. Guo, "Actively controllable terahertz switches with graphene-based nongroove gratings," *Photon. Res.*, vol. 5, no. 6, pp. 604–611, Dec. 2017.

[37] S. K. Ghosh, V. S. Yadav, S. Das, and S. Bhattacharyya, "Tunable graphene-based metasurface for polarization-independent broadband absorption in lower mid-infrared (MIR) range," *IEEE Trans. Electromagn. Compat.*, vol. 62, no. 2, pp. 346–354, Apr. 2020.

[38] V. S. Yadav, S. K. Ghosh, S. Das, and S. Bhattacharyya, "Wideband tunable mid-infrared cross-polarisation converter using monolayered graphene-based metasurface over a wide angle of incidence," *IET Microw., Antennas Propag.*, vol. 13, no. 1, pp. 82–87, Jan. 2019.

[39] V. S. Yadav, S. K. Ghosh, S. Bhattacharyya, and S. Das, "Graphene-based metasurface for a tunable broadband terahertz cross-polarization converter over a wide angle of incidence," *Appl. Opt.*, vol. 57, no. 29, pp. 8720–8726, Oct. 2018.

[40] M. Wang, Q. Zeng, L. Deng, B. Feng, and P. Xu, "Multifunctional graphene metasurface to generate and steer vortex waves," *Nanosc. Res. Lett.*, vol. 14, no. 1, p. 343, Nov. 2019.

[41] S. E. Hosseininejad, K. Rouhi, M. Neshat, A. Cabellos-Aparicio, S. Abadal, and E. Alarcon, "Digital metasurface based on graphene: An application to beam steering in terahertz plasmonic antennas," *IEEE Trans. Nanotechnol.*, vol. 18, pp. 734–746, 2019.
[42] J.-Y. Liu, T.-J. Huang, and P.-K. Liu, "Tunable polarization-independent terahertz band-stop filter based on graphene metasurface," in *Proc. 43rd Int. Conf. Infr., Millim., Terahertz Waves (IRMMW-THz)*, Nagoya, Japan, Sep. 2018, pp. 1–2.
[43] O. Balci, N. Kakenov, E. Karademir, S. Balci, S. Cakmakyapan, E. O. Polat, H. Caglayan, E. Özbay, and C. Kocabas, "Electrically switchable metadevices via graphene," *Sci. Adv.*, vol. 4, no. 1, Jan. 2018, Art. no. eaao1749.
[44] B. Xiao, Y. Zhang, S. Tong, J. Yu, and L. Xiao, "Novel tunable graphene-encoded metasurfaces on an uneven substrate for beam-steering in far-field at the terahertz frequencies," *Opt. Express*, vol. 28, no. 5, pp. 7125–7138, Feb. 2020.
[45] B. Xiao, S. Tong, A. Fyffe, and Z. Shi, "Tunable electromagnetically induced transparency based on graphene metamaterials," *Opt. Express*, vol. 28, no. 3, pp. 4048–4057, Jan. 2020.
[46] S. Gong, B. Xiao, L. Xiao, S. Tong, S. Xiao, and X. Wang, "Hybridization-induced dual-band tunable graphene metamaterials for sensing," *Opt. Mater. Express*, vol. 9, no. 1, pp. 35–43, Jan. 2019.
[47] T. Jiang, D. Huang, J. Cheng, X. Fan, Z. Zhang, Y. Shan, Y. Yi, Y. Dai, L. Shi, K. Liu, C. Zeng, J. Zi, J. E. Sipe, Y. R. Shen, W. T. Liu, and S. Wu, "Gate-tunable third-order nonlinear optical response of massless Dirac fermions in graphene," *Nature Photon.*, vol. 12, no. 7, pp. 430–436, May 2018.
[48] G. Soavi, G. Wang, H. Rostami, D. G. Purdie, D. De Fazio, T. Ma, B. Luo, J. Wang, A. K. Ott, D. Yoon, S. A. Bourelle, J. E. Muench, I. Goykhman, S. Dal Conte, M. Celebrano, A. Tomadin, M. Polini, G. Cerullo, and A. C. Ferrari, "Broadband, electrically tunable third-harmonic generation in graphene," *Nature Nanotechnol.*, vol. 13, no. 7, pp. 583–588, Jul. 2018.
[49] J. Li, T. Zhang, and L. Chen, "High-efficiency plasmonic third-harmonic generation with graphene on a silicon diffractive grating in mid-infrared region," *Nanosc. Res. Lett.*, vol. 13, no. 1, p. 338, Oct. 2018.
[50] Y. Fan, N.-H. Shen, F. Zhang, Q. Zhao, Z. Wei, P. Zhang, J. Dong, Q. Fu, H. Li, and C. M. Soukoulis, "Photoexcited graphene metasurfaces: Significantly enhanced and tunable magnetic resonances," *ACS Photon.*, vol. 5, no. 4, pp. 1612–1618, Feb. 2018.
[51] F. Xiao, W. Zhu, W. Shang, T. Mei, M. Premaratne, and J. Zhao, "Electrical control of second harmonic generation in a graphene-based plasmonic Fano structure," *Opt. Express*, vol. 23, no. 3, pp. 3236–3244, Feb. 2015.
[52] V. P. Gusynin, S. G. Sharapov, and J. P. Carbotte, "Magneto-optical conductivity in graphene," *J. Phys., Condens. Matter*, vol. 19, no. 2, Dec. 2006, Art. no. 026222.
[53] P.-Y. Chen and A. Alú, "Atomically thin surface cloak using graphene monolayers," *ACS Nano*, vol. 5, no. 7, pp. 5855–5863, Jun. 2011.
[54] Z. Q. Li, E. A. Henriksen, Z. Jiang, Z. Hao, M. C. Martin, P. Kim, H. L. Stormer, and D. N. Basov, "Dirac charge dynamics in graphene by infrared spectroscopy," *Nature Phys.*, vol. 4, no. 7, pp. 532–535, Jun. 2008.
[55] K. I. Bolotin, K. J. Sikes, Z. Jiang, M. Klima, G. Fudenberg, J. Hone, P. Kim, and H. L. Stormer, "Ultrahigh electron mobility in suspended graphene," *Solid State Commun.*, vol. 146, nos. 9–10, pp. 351–355, Jun. 2008.
[56] A. Vakil and N. Engheta, "Transformation optics using graphene," *Science*, vol. 332, no. 6035, pp. 1291–1294, Jun. 2011.
[57] Y. Wang, T. Li, and S. Zhu, "Graphene-based plasmonic modulator on a groove-structured metasurface," *Opt. Lett.*, vol. 42, no. 12, pp. 2247–2250, Jun. 2017.
[58] T. Ren and L. Chen, "Slow light enabled high-modulation-depth graphene modulator with plasmonic metasurfaces," *Opt. Lett.*, vol. 44, no. 22, pp. 5446–5449, Nov. 2019.
[59] M. A. Ordal, L. L. Long, R. J. Bell, S. E. Bell, R. R. Bell, R. W. Alexander, and C. A. Ward, "Optical properties of the metals Al, Co, Cu, Au, Fe, Pb, Ni, Pd, Pt, Ag, Ti, and W in the infrared and far infrared," *Appl. Opt.*, vol. 22, no. 7, pp. 1099–1119, Apr. 1983.
[60] K. O'Brien, H. Suchowski, J. Rho, A. Salandrino, B. Kante, X. Yin, and X. Zhang, "Predicting nonlinear properties of metamaterials from the linear response," *Nature Mater.*, vol. 14, no. 4, pp. 379–383, Feb. 2015.
[61] J. Butet and O. J. F. Martin, "Evaluation of the nonlinear response of plasmonic metasurfaces: Miller's rule, nonlinear effective susceptibility method, and full-wave computation," *J. Opt. Soc. Amer. B, Opt. Phys.*, vol. 33, no. 2, pp. A8–A15, Feb. 2016.
[62] N. P. Armitage, R. Tediosi, F. Lévy, E. Giannini, L. Forro, and D. van der Marel, "Infrared conductivity of elemental bismuth under pressure: Evidence for an avoided lifshitz-type semimetal-semiconductor transition," *Phys. Rev. Lett.*, vol. 104, no. 23, Jun. 2010, 237401.
[63] J. Yao, G. Cai, N. Liu, and Q. H. Liu, "Enhancing artificial sum frequency generation from graphene-gold metamolecules," *Opt. Lett.*, vol. 43, no. 13, pp. 3160–3163, Jul. 2018.
[64] C.-F. Chen, C.-H. Park, B. W. Boudouris, J. Horng, B. Geng, C. Girit, A. Zettl, M. F. Crommie, R. A. Segalman, S. G. Louie, and F. Wang, "Controlling inelastic light scattering quantum pathways in graphene," *Nature*, vol. 471, no. 7340, pp. 617–620, Mar. 2011.
[65] Z. Wu, Y. Han, R. Huang, X. Chen, Y. Guo, Y. He, W. Li, Y. Cai, and N. Wang, "Semimetallic-to-metallic transition and mobility enhancement enabled by reversible iodine doping of graphene," *Nanoscale*, vol. 6, no. 21, pp. 13196–13202, 2014.
[66] A. Tomadin, S. M. Hornett, H. I. Wang, E. M. Alexeev, A. Candini, C. Coletti, D. Turchinovich, M. Kläui, M. Bonn, F. H. L. Koppens, E. Hendry, M. Polini, and K.-J. Tielrooij, "The ultrafast dynamics and conductivity of photoexcited graphene at different Fermi energies," *Sci. Adv.*, vol. 4, no. 5, May 2018, Art. no. eaar5313.
[67] R. Feng, J. Qiu, L. Liu, W. Ding, and L. Chen, "Parallel LC circuit model for multi-band absorption and preliminary design of radiative cooling," *Opt. Express*, vol. 22, no. S7, pp. A1713–A1724, Dec. 2014.
[68] Q. Guo, C. Li, B. Deng, S. Yuan, F. Guinea, and F. Xia, "Infrared nanophotonics based on graphene plasmonics," *ACS Photon.*, vol. 4, no. 12, pp. 2989–2999, Aug. 2017.

KAI GUO received the B.S. degree in applied physics and the Ph.D. degree in physics from the Harbin Institute of Technology, Harbin, China, in 2010 and 2015, respectively. From 2015 to 2016 and from 2016 to 2017, he was a Postdoctoral Research Fellow with Sungkyunkwan University, Suwon, South Korea, and Hongkong Polytechnic University, Hongkong, respectively. He is currently working as an Assistant Professor with the Hefei University of Technology, Hefei, China. His research interests include theoretical surface plasmonics, light manipulation with metamaterials and metasurfaces, and nonlinear optics.

ZIXIANG LI received the B.S. degree in photoelectric information engineering from Xian Technology University at Xian, Xian, China, in 2014. He is currently pursuing the M.S. degree with the Advanced Electromagnetism Function Laboratory (AEMFLab), Hefei University of Technology. His research interests are mainly in the metasurface and artificial second harmonic generation.

ZHONGYI GUO received the bachelor's, master's, and Ph.D. degrees from the Department of Physics, Harbin Institute of Technology, in 2003, 2005, and 2008, respectively. Then, he continued to work in the Harbin Institute of Technology. From 2008 to 2009, he worked as an Assistant Professor with the Department of Physics, Harbin Institute of Technology. Then, he moved to Hanyang University, South Korea and worked as a Postdoctor for two years. In 2011, he continued to move to The Hong Kong Polytechnic University as a Postdoctor for six months. In the end of 2011, he joined in and worked as a Full Professor at the School of Computer and Information, Hefei University of Technology. He currently focus his research interests in the fields of advanced optical communication, OAM antenna, polarization information processing, manipulation of optical fields, and nanophotonics.